Filtering of Nanoparticles with Tunable Semiconductor Membranes

Anna Nadtochiy, Dmitriy Melnikov, and Maria Gracheva*

Department of Physics, Clarkson University, 8 Clarkson Avenue, Potsdam, New York 13699, United States

ABSTRACT Translocation dynamics of nanoparticles permeating through the nanopore in an *n*-Si semiconductor membrane is studied. With the use of Brownian Dynamics to describe the motion of the charged nanoparticles in the self-consistent membrane-electrolyte electrostatic potential, we asses the possibility of using our voltage controlled membrane for the macroscopic filtering of the charged nanoparticles. The results indicate that the tunable local electric field inside the membrane can effectively control interaction of a nanoparticle with the nanopore by either blocking its passage or increasing the translocation rate. The effect is particularly strong for larger nanoparticles due to their stronger interaction with the membrane while in the nanopore. By extracting the membrane permeability from our microsopic simulations, we compute the macroscopic sieving factors and show that the size selectivity of the membrane can be tuned by the applied voltage.

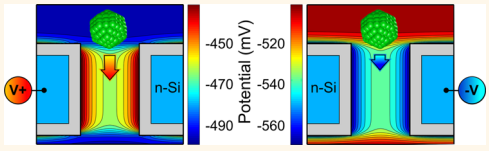

KEYWORDS: nanopore · nanoparticle · semiconductor membrane · filtering · Brownian Dynamics

The separation of similarly sized objects is an important problem in biomedical research as well as in technological purification of biomolecules and nanoparticles. Compared to standard chromatography methods of separation, sample purification methods based on the membrane technologies are more efficient as they allow for in principle continuous filtering process. However, traditional filtering membranes made from polymers frequently suffer from low membrane permeability to the filtered objects, clogging, and sample loss due to the long channels and large pore size distributions.[1]

Modern day nanotechnology enables creation of artificial nanoporous membranes made of a variety of materials by various methods. In these membranes, all nanopore characterisitcs, its length and diameter distribution as well as the sample porocity and membrane surface chemistry, can be controlled with high accuracy, thus enabling their applications for single molecule sensing and filtration.[2−7] For example, the pores can be made as small as 1 nm in diameter making it potentially suitable for sequencing DNA molecules.[8]

One of the most versatile type of membranes are semiconductor membranes[9,10] which could consist of one or several layers of the doped Si.[10,11] In addition to the control over the geometric characteristics of pores, they also allow for the control of the local electrostatic potential distribution. This is achieved by applying voltage to the membrane layers, thus changing the potential inside the membrane and in the vicinity of the nanopore. Originally, these membranes were studied for the tunable control over the DNA translocation.[12] In this work, we broaden the scope and consider the possibility of applying these membranes to tunable filtering and separation of nanoparticles and proteins.

Specifically, we perform numerical analysis of a negatively charged nanoparticle translocation through the nanopore created in the nanometer-thin, heavily n-doped Si membrane. We use Brownian Dynamics approach to describe the motion of the nanoparticles in the self-consistent electroststic field produced by all charges (membrane and electrolyte) in the system subjected to the membrane bias. On the bases of these microscopic simulations, we then asses the possibility to utilize our voltage controlled membrane for the macroscopic filtering of the charged nanoparticles. By changing the membrane voltage, we show that the sieving factor of such a membrane filter and the filtering time can be changed by the order of magnitude.

The results and methods presented in our work also provide a bridge between the microscopic simulations of individual macromolecules such as proteins or nanoparticles,[13−15] which do not account for the

* Address correspondence to gracheva@clarkson.edu.

Received for review May 10, 2013 and accepted July 23, 2013.

Published online July 23, 2013
10.1021/nn4023697

macroscopic filtering mechanisms, and a macroscopic continuum modeling of the flow of these objects through nanoporous membranes,[16−18] which does not take into account effects of the local environment of the filtered particles. Even though in this work we focus on the doped Si membrane, our results can also be applied to other voltage controlled membranes such as those made from graphene[19−21] or based on the local electrostatic control using nanowires[22] or nanotubes.[23] Our method of characterization of the membrane filtering properties can also be easily adapted to the dielectric membranes such as those made of SiN[4,5] or polynanocrystalline (pnc)-Si.[2]

RESULTS AND DISCUSSION

Electrostatic Potential. The distribution of the electrostatic potential obtained from the self-consistent solution of the Poisson equation (9) is shown in Figure 1. Since there is no applied electrolyte bias, the potential is symmetric with respect to the membrane center (x = 130 Å). One can also see that for the positive membrane bias (Figure 1A), the potential is higher than its asymptotic value in the bulk of the electrolyte where the effects of the membrane charges and voltage are screened off by the solution charges. This is because the application of the large positive bias on the membrane depletes the mobile charges (electrons in this case), thus leaving the membrane positively charged (due to the donor ions in the semiconductor layer). This large positive charge, partially screened by the negative surface charge, is nevertheless strong enough to produce a larger than the bulk potential within the confined nanopore volume. The positive charge in the membrane also attracts negatively charged nanoparticles as if the nanopore diameter increases beyond its geometrical value (the capture rate increases).

For the negative membrane bias case, $V_m = -1$ V, shown in Figure 1B, the large negative voltage on the membrane allows for the almost complete compensation of the charges within the membrane, thus leaving only the surface charge as the sole membrane charge. (This potential is very similar to the one for the conventional SiO_2 membrane, for comparison see Figure 1 in Supporting Information.) This negative charge repels negatively charged nanoparticles, so that effectively, the diameter of the nanopore decreases below its geometric diameter (the capture rate decreases). Because of the different values of the donor concentration in the semiconductor and the surface charge density (N_D and N_s, respectively, see Method) and their spatial distributions, the potential changes at $V_m = \pm 1$ V are slightly asymmetric with respect to the bulk potential. Note also that the variation of the potential along the nanopores cross section (along the z-direction) is also consistent with these interpretations: the potential increases (decreases) toward the nanopore surface for $V_m = 1$ (−1) V.

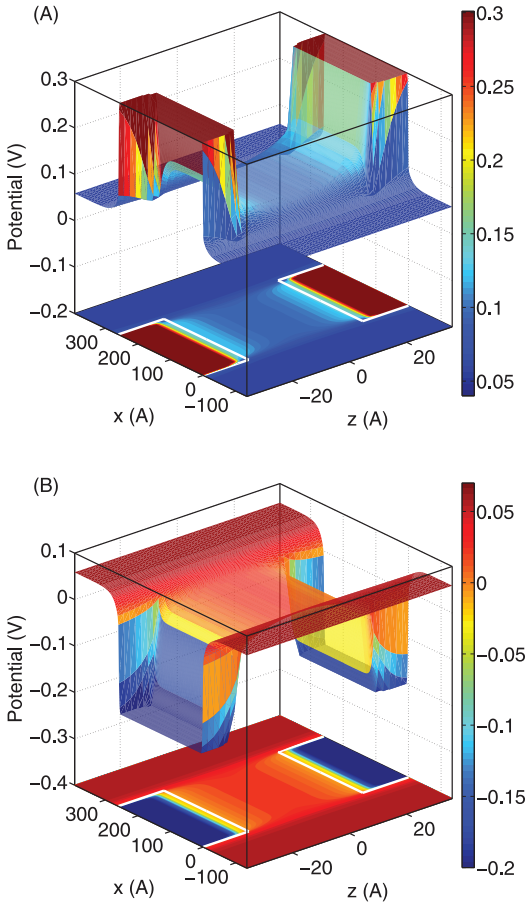

Figure 1. Electrostatic potential $\varphi(\vec{r})$ for (A) $V_m = 1$ V and (B) $V_m = -1$ V. Note that, in order to emphasize the details of the potential distribution in the nanopore, the potential is cut off at 0.3 V in (A) and −0.2 V in (B). The membrane outline is shown in white.

This effect of the charge inversion, which was discussed by us earlier,[24] modifying the effective diameter of the pore opening (and thus, its capture rate) is the basis of our tunable filtering mechanism of nanometer-sized particles as described below. As we do not apply in this work the electrolyte bias, the possible mechanism of the filtering is the differential equilibration rates or applying the pressure difference.

Translocation Dynamics of a Nanoparticle. In this section, we analyze the translocation of a charged nanoparticle through the nanopore when no electrolyte bias is applied. In this case, the particle diffuses in the potentials shown in Figure 1. For each membrane voltage, we study the translational Brownian Dynamics (BD) of nanoparticles with radii 4−16 Å. Before each simulation, the nanoparticle is placed in the bounding volume (see Figure 7) so that its center of mass is 40 Å above the pore's entrance. From the analysis of the particle trajectories (≈10^3 simulations for each case), we extract the time which the particle spends above the pore in the bounding volume before it enters the pore and successfully translocates to the other end (the

waiting times, τ_w), and time necessary to translocate through the pore (the translocation or the dwell time, τ_t). The histograms of the waiting time distributions are shown in Figure 2 for three different nanoparticle sizes and membrane voltages $V_m = \pm 1$ V. As expected, the smaller the radius of the particle, the less time it spends finding the pore (smaller τ_w), but these times are very much different for $V_m = \pm 1$ V.

The underlying physical mechanism describing the behavior of the nanoparticle is that of a particle diffusing in the solution attempting first to locate the nanopore and then successfully permeate it.[25] This mechanism is similar in the essence to the process of diffusion of a particle initially confined to a volume V_b and trying to exit through a hole of a small diameter. Such processes were extensively studied in view of their importance in determination of the time scale of excitations observed in dendritic spines, the sites where synapses are located in neurons.[26] The dendritic spines can be schematically represented by a large head of volume V_b with a thin long neck of length L_m and diameter D_{pore} ($L_m \gg D_{pore}$) through which signaling molecules can escape. With the help of the BD simulations, it was shown[26,27] that the time for the particle to stay in the head of the dendritic spine (the "survival time") is[28]

$$\tau_w \approx \frac{\xi}{k_B T}\left[\frac{4 L_m V_b}{\pi D_{pore}^2}\right] \quad (1)$$

On the other hand, a molecule in the head of the dendritic spine tunneling through its long neck to escape is similar to the setup of our BD simulations where we initially confine the nanoparticle in the large volume above the long and narrow nanopore and then let it find the pore's entrance and permeate the membrane, *cf.* Figure 7 of the present work with, for example, Figure 1 in ref 27 or Figure 2e in ref 29. It also follows from these works that the survival probability (which in our case is the probability for a particle to enter the pore at a time t and successfully permeate it) has a single exponential dependence $\exp(-t/\tau_w)$ on time. As one can see from Figure 2, our computed distributions are in excellent agreement with this dependence.

We should also emphsize that similar single exponential dependence was recently observed in experimental study of the time intervals between translocation events for nanoparticles.[5] In ref 5, this decay was interpreted as a consequence of the absence of interaction between the particles when, at the sufficiently low density, they translocate through the nanopore one by one without competition. In our simulations, we also consider translocations of individual particles assuming that once a particle is gone, another one immediately appears in the bounding volume, and the process repeats. In this interpretation, the bounding volume is equal to the volume per one particle which gives us the concentration of filtering particles of about 30 μM.

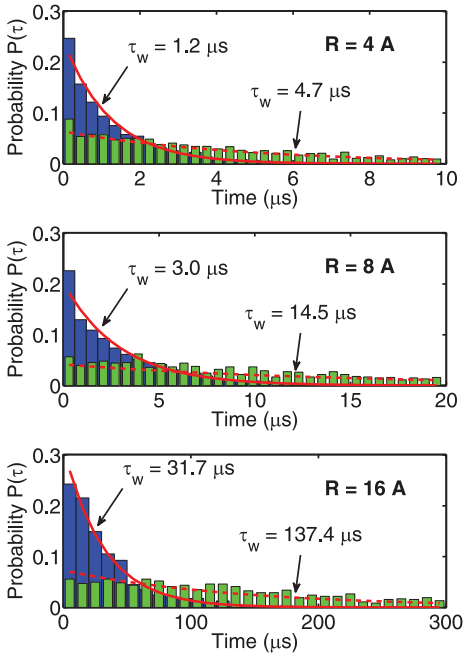

Figure 2. Histograms of the waiting time distributions $P(t)$ for the nanoparticle radii 4, 8, and 16 Å and for $V_m = 1$ V (blue) and $V_m = -1$ V (green). Red curves show the envelope probability density function $\tau_w^{-1} \exp(-t/\tau_w)$, see text for discussion.

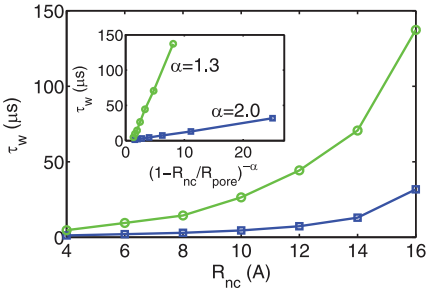

Figure 3. Waiting times τ_w *vs* nanoparticle radius R_{nc} for $V_m = 1$ V (blue) and $V_m = -1$ V (green). Inset shows that the $\tau_w \propto (1 - 2R_{nc}/D_{pore})^{-\alpha}$ in the studied range of particle sizes. With the use of linear extrapolation, this dependence allows us to extract values of τ_w for larger R_{nc} which would otherwise be difficult to accurately compute: for example, we obtain $\tau_w \sim 400$ μs for $R_{nc} = 18$ Å at $V_m = -1$ V.

The waiting times, τ_w, for different R_{nc} and V_m are shown in Figure 3. As one can see, the larger the size of the particle, the stronger the influence which the membrane exerts on its dynamics. The differences in values become especially pronounced for larger R_{nc}: for example, for 16 Å radius, τ_w is almost 5 times smaller for $V_m = 1$ V case than for -1 V. This is because of the increased effective diameter of the pore due to the strong electric field near the entrance to the pore (see Figure 1), which enhances the rate with which particles are captured. For the negative membrane bias, the electric field near the entrance repels the particles

away from the pore and they have to spend much longer time inside the bounding volume and make a larger number of attempts to translocate through the pore. These large differences in the waiting time values also drastically affect the permeability of the membrane as discussed in the following section where it is shown that this quantity can be controlled by the bias voltage applied to the membrane.

The dependence of the translocation time τ_t (determined as the difference between the time the particle enters the pore and the time it emerges at the other end without re-entering) on the nanoparticle radius and membrane voltage is presented in Figure 4. It is seen that these dependencies have linear character, *i.e.*, $\tau_t \propto R_{nc}$. This is easily explained within the one-dimensional diffusion model of the conditional mean first passage time,[30] according to which $\tau_t = L_p^2/(6D)$ where $D = k_BT/\xi = k_BT/(6\pi\eta R_{nc})$ is the nominal diffusion coefficient of the spherical particle with radius R_{nc}. This dependence is shown by the red line in Figure 4. While in the nanopore, the particle's interaction with it depends on the applied membrane voltage which modifies the electrostatic potential profile in it (Figure 1). This results in different effective diffusion coefficients. By fitting the computed data with the results of the simple diffusion model, we find that the computed values of τ_t for the positive (negative) membrane bias correspond to the 15% decrease (increase) in the drag coefficient, so that it takes longer (shorter) amount of time for it to translocate through the nanopore. In other words, as can be seen from Figures 3 and 4, at $V_m = -1$ V it takes longer for the particle to get to the pore, but once in the pore, it translocates faster. Although not central to the purpose of the work, this correlation between the translocation and waiting times is reminiscent of a recent experimental work on optimization of the particle transport through synthetic nanopores where the potential inside the channel was modulated with the laser tweezers.[31]

Filtering of Nanoparticles. Although the drastically different values of the waiting times for $V_m = \pm 1$ V shown in Figure 3 already indicate that the rate with which particles penetrate through the membrane strongly depends on the applied membrane voltage, by themselves, they do not describe the complete membrane filtering process. Indeed, this process depends also on the macroscopic diffusion of particles from the *cis* (retentate) chamber toward the membrane. If this process is very slow, with the time scale much larger that either of the waiting times in Figure 3, the membrane will play little role in hindering the flow of these particles. As such, to describe macroscopic filtering of particles, we need to compare the effective resistance offered by the membrane with the resistance of the fluid chamber filled with nanoparticles. In the simple one-dimensional model, the latter one is

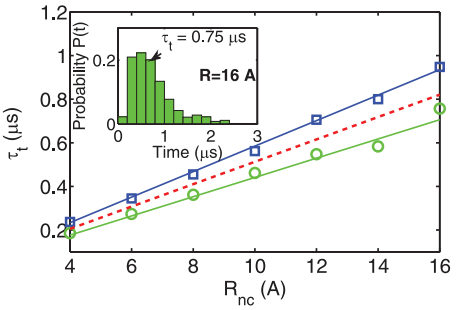

Figure 4. Translocation time τ_t *vs* R_{nc} for $V_m = 1$ V (blue) and $V_m = -1$ V (green). Symbols show the average values computed from the translocation time distributions (an example histogram for $R_{nc} = 16$ Å is shown in the inset); the solid lines show the dependencies computed from the diffusion model with fitted values of the diffusion coefficient. The red dashed line is the theoretical dependence calculated for the nominal diffusion coefficient k_BT/ξ.

given by $\Omega_c = \xi W/k_BT$ where W is the length of the chamber. The membrane resistance (the inverse permeability) was shown[17,32] to be dependent on the membrane thickness L_m, the pore's diameter D_{pore}, the diffusion coefficient k_BT/ξ of nanoparticles in the retentate chamber, and the porocity of the membrane N (the number of pores per unit area). In the limit of $L_m \gg D_{pore}$, it is given by:

$$\Omega_m \approx \frac{\xi}{k_BTN}\left[\frac{4L_m}{\pi D_{pore}^2}\right] \qquad (2)$$

With help of eq 1, we can rewrite the above equation as

$$\Omega_m = \frac{\tau_w}{NV_b} \qquad (3)$$

thus relating the macroscopic membrane resistance Ω_m to the microscopic waiting time τ_w and the pore density (membrane porosity). Note that N can be varied in the broad range from 1 to 10^9 pores per cm^2.[33]

The computed in this way values of the membrane Ω_m and the chamber Ω_c resistances as well as their ratio $\beta = \Omega_m/\Omega_c$ as functions of the translocating nanoparticle radius are shown in Figure 5 for the same two membrane voltages $V_m = \pm 1$ V as in the previous plots. One can see that the membrane resistance increases as the particle gets larger as expected since it becomes more difficult for a large nanoparticle to enter the pore in order to achieve a successful translocation. Also, because the waiting time is smaller for $V_m = 1$ V, the membrane resistance is also weaker for the same R_{nc} value. It is also interesting to note that for our membrane parameters, Ω_c (red line in Figure 5) is actually smaller than Ω_m for the majority of the particles (it is multiplied by 10 in Figure 5 for clarity), except for small R_{nc} at $V_m = 1$ V when they are comparable, which means that the membrane resistance is almost always dominant ($\beta \gg 1$, see inset in Figure 5).

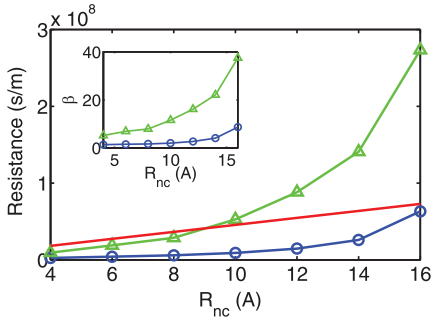

Figure 5. Membrane (curves with symbols) and chamber (red line) resistances computed from eq 3 *vs* the radius of the nancrystals R_{nc} for $V_m = 1$ V (blue curve) and -1 V (green curve). Ω_c values are multiplied by 10 to bring them up to the scale of the plot. Inset shows the ratio $\beta = \Omega_m/\Omega_c$ *vs* R_{nc}. For these calculation,s we took the chamber size W = 1 mm[17] and the pore density $N = 10^8$ cm^{-2}.[33]

To find how concentration $c(x,t)$ of nanoparticles changes in both retentate and filtrate chambers during the filtration, we analytically solve the one-dimensional diffusion equation in the x-direction along the nanopore axis[17,34]

$$\frac{\partial c}{\partial t} = \frac{k_B T}{\xi_t}\frac{\partial^2 c}{\partial x^{2'}} \qquad -W < x < W \tag{4}$$

where initially all nanoparticles are located in the retentate chamber to the left of the membrane, *i.e.*, $c(x < 0,t = 0) = c_0$ and $c(x > 0,t = 0) = 0$.

Assuming that the membrane thickness is much smaller than the size of the filtration chamber, for the concentration change across the membrane (at $x = 0$), we write

$$\left.\frac{k_B T}{\xi}\frac{\partial c}{\partial x}\right|_{x=0} = \Omega_m^{-1}(c_r - c_l) \tag{5}$$

where $c_{r(l)}$ is the concentration in the filtrate (retentate), respectively.

The solution to this boundary-value problem can be written as

$$c(x,t) = c_0\left[\frac{1}{2} + \sum_{n=0}^{\infty}\frac{\sin\lambda_n}{\lambda_n + \cos\lambda_n \sin\lambda_n}\chi_n(x) \times \exp\left(-\frac{kT\lambda_n^2 t}{\xi W^2}\right)\right] \tag{6}$$

$$\chi_n(x) = \begin{cases} \cos\left[\frac{\lambda_n}{W}(x - W)\right], & -W < x < 0 \\ -\cos\left[\frac{\lambda_n}{W}(x + W)\right], & 0 < x < W \end{cases} \tag{7}$$

$$\tan\lambda_n = \frac{2}{\beta\lambda_n} \tag{8}$$

One can see from the last equation that the ratio of the membrane and chamber resistances β, see Figure 5, determines the values of the eigenvalues λ_n. In particular, in the limit of $\beta \gg 1$, $\lambda_n \approx (2/\beta)^{1/2} + \pi n$, so that the characteristic time of the concentration change, given by the leading term with $n = 0$ in eq 6, is $\sim \Omega_m W/2$.

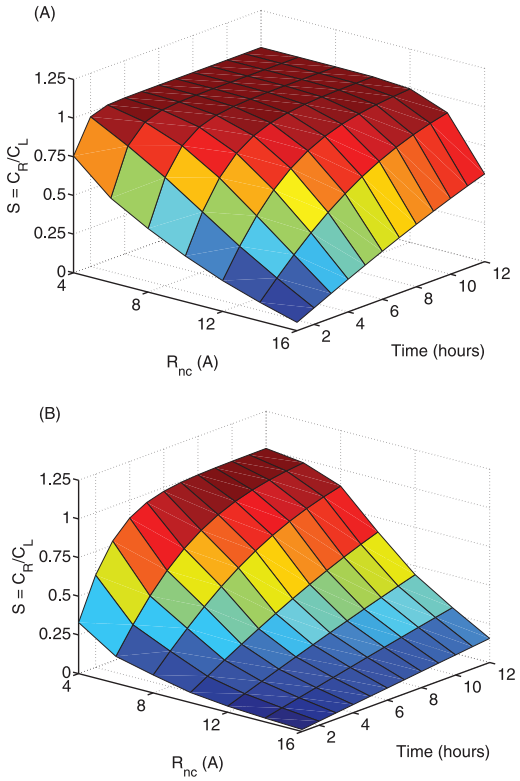

Figure 6. Sieving factor S for different nanoparticle radii R_{nc}, filtration times, and membrane voltages: (a) $V = 1$ V, (b) $V = -1$ V.

To see how nanoparticle concentration increases in the filtrate chamber (which is initially empty) during the filtration process, we study the time dependence of the sieving factor S defined as the ratio of the average concentrations to the right C_R and to the left C_L of the membrane, $S(t) = C_R/C_L$. This quantity is plotted in Figure 6 for different radii of the nanoparticles R_{nc}, membrane voltages $V_m = \pm 1$ V, and filtration times. One can see from this plot that for the positive membrane voltage the sieving factor is always larger for the same filtration times and nanoparticle sizes. This is because of the smaller membrane resistance in this case (see Figure 5) which means that the particles permeate the membrane faster and their concentrations equalize sooner. One can also notice that larger nanoparticles permeate slower so that S for them is also smaller. This allows for the filtering of the particles by size: for example, at $V_m = -1$ V and filtration time of 12 h, the sieving factor for the 16 Å particles is about 10 times smaller than that for 4 Å ones, which means that the concentration of these particles in the filtrate chamber is 10 times smaller than in the retentate.

This plot also demonstrates the range of the filtering tunability offered by our membrane. For example, when $V_m = -1$ V, 4 and 16 Å particles can be easily separated after 4 h (see Figure 6B) since, at this time, the sieving

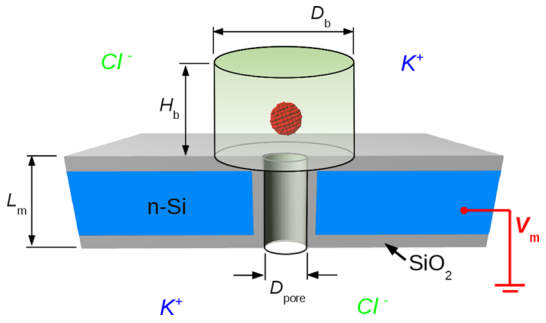

Figure 7. Schematic representation of the simulated system. To initiate translocation, a nanoparticle is placed in the bounding box with dimensions H_b = 10 nm, D_b = 8 nm positioned atop the nanopore. This volume corresponds to the concentration of the nanoparticles of 30 μM.

coefficients are $S \sim 1$ and $S \sim 0.1$ for $R_{nc} = 4$ Å and 16 Å, respectively. However, to achieve the noticeable separation between, for example, 10 and 16 Å particles at that filtering time or earlier, we need to change the membrane voltage to V_m = 1 V. Then, at 4 h, the sieving factors for these sizes are ~1 and ~0.2 (Figure 6A), whereas in order to reach the same values of S when $V_m = -1$ V, one has to wait for more than 12 h.

We should also note the versatility of our membrane which can be equally well used for various geometries of the filtration systems. The filtering chamber length W is usually defined by the problem at hand, and by changing V_m, we can modify the membrane resistance Ω_m and the sieving coefficients to compensate (in order to have the same characteristic filtering time $\sim \Omega_m W$) and thus ensure the maximum possible separation rate and quality.

CONCLUSION

In this work, we considered the translocation of the charged spherical nanoparticles of variable radii through the nanoporous semiconducting membrane in order to study the possibility of the tunable filtering of these objects. To gain insight into the microscopic dynamics of the nanoparticles, we utilized the coarse-grained Brownian Dynamics technique to describe the motion of a nanoparticle in the self-consistent electrostatic potential created by the charges in the membrane and electrolyte as well as the applied membrane voltage. The results of these simulations, particularly, the times which nanoparticles spend trying to locate the pore, were then applied to evaluate the membrane resistance in order to study the continuous flow of the particles within a diffusion approximation. This macroscopic approach allowed us to calculate particle concentration changes and extract sieving factors characterizing the filtering properties of our membrane.

We found that application of different membrane voltages greatly changes the permeability of the membrane as the membrane charge in the vicinity of the nanopore can either attract the charged nanoparticles to the channel thereby decreasing the membrane resistance or repel them. This electrostatic blocking or opening of the nanopore has direct repercussions on the filtration of particles as it becomes possible with our voltage controlled membrane to greatly vary the filtering selectivity to the size of nanoparticles as well as the filtration rate (both by a factor of 10).

In this work, we assessed the filtering capabilities of our membrane when the nanometer sized particle dynamics is affected only by the membrane charges and voltages, *i.e.*, we kept the electrolyte bias at zero. When the electrolyte bias is applied, one would expect that the differences in waiting times and membrane resistances observed for different membrane biases will be washed out as the charged particles will move along the electric field in the nanopore (electrophoresis) produced by this bias, which could be strong compared to the field from the membrane charges. The electrostatic mechanism will probably be also diminished in importance in larger pores as there will be more room for the electrolyte charges to screen out the membrane charges. However, when the electrolyte bias is applied, another transport mechanism appears due to the electroosmotic flow in the nanopore area. It exerts additional drag force on the nanoparticle, and the larger the particle, the stronger the force, so that in larger pores it cannot be neglected. For the positive membrane bias, when the nanopore is filled with Cl^- ions, this flow should carry the nanoparticle to the membrane so that it will be captured faster (membrane permeability increases). On the other hand, for the negative bias, the flow is predominantly due to the potassium ions, which move in the opposite direction and push the nanoparticle away from the pore (membrane permeability decreases).

Previously similar mechanism of the reversal of the electroosmotic flow was theoretically discussed[35] in connection with slowing down DNA in the nanopore, and recent experimental study[36] also showed that the flow can also be controlled by changing pH of the solution. The *inversion* of the electroosmotic flow direction considered in this work is the unique feature of our *n*-Si membrane with its voltage tunable effective charge,[24] and its effects on the filtering of larger macromolecules such as proteins will be discussed in our subsequent works.

METHOD

Simulated Structure. Our simulated system is schematically shown in Figure 7. We consider a cylindrical nanopore with diameter D_{pore} = 4 nm in the 26-nm-thick semiconductor membrane (L_m = 26 nm) consisting of a 24-nm-thick layer of the *n*-doped Si material covered by a 1 nm-thick layer of silicon

dioxide SiO_2.[10] The membrane is immersed in an electrolyte solution (KCl) with concentration $C_{KCl} = 0.05$ M corresponding to the Debye screening length $L_D \approx 1.3$ nm. Since $2L_D < D_{pore}$, we can apply the continuum approach to describe electrostatic potential and charge distribution in our membrane−electrolyte structure as it was done in previous studies.[37,38]

Electrostatics. The charges in the membrane and the electrolyte as well as the applied external biases create the electrostatic potential $\varphi(\vec{r})$ in the system, in which the simulated particle then moves. To find this potential, we solve the Poisson equation[39]

$$\nabla[\varepsilon(\vec{r})\nabla\varphi(\vec{r})] = -\rho(\vec{r}) \quad (9)$$

with the device boundary conditions, *i.e.*, the normal component of the electric field is zero on the lateral surfaces of the simulated volume and the potential φ is constant on the top and bottom ones (above and below membrane). In eq 9, $\rho(\vec{r})$ is the charge density, $\varepsilon(\vec{r}) = \varepsilon_0\varepsilon_r(\vec{r})$, and the dielectric permittivity $\varepsilon_r = 11.7$ for Si, 3.9 for SiO_2, and 78 for the electrolyte (ε_0 is the permittivity of the free space).

The charge density $\rho(\vec{r})$ in the *n*-Si membrane is

$$\rho(\vec{r}) = -e[n(\vec{r}) - N_D^+(\vec{r}) + N_s(\vec{r})] \quad (10)$$

where $n(\vec{r})$ is the concentration of electrons which obeys Fermi-Dirac statistics[40] with the Fermi level that is shifted by eV_m. $N_D^+(\vec{r}) = 2 \times 10^{20}$ cm^{-3} is the donor density in the semiconductor, whereas $N_s(\vec{r}) = 4 \times 10^{20}$ cm^{-3} represents the density of the fixed surface charge in the SiO_2 layer on the membrane. To model the interface between the membrane and the electrolyte, we also use the offsets between the conduction bands of 3.2 eV for SiO_2 and −0.3 V for electrolyte with respect to Si.[10]

The charge density $\rho(\vec{r})$ in the electrolyte is given by

$$\rho(\vec{r}) = e[C_{K^+}(\vec{r}) - C_{Cl^-}(\vec{r})] \quad (11)$$

At room temperature, the electrolyte is a fully dissociated KCl so that in the absence of an external potential $C_{K^+} = C_{Cl^-} = C_{KCl}$. At equilibrium, when no bias is applied to the electrolyte, concentrations of potassium and chlorine ions, $C_{K^+}(\vec{r})$ and $C_{Cl^-}(\vec{r})$, in eq 11 obey Boltzmann statistics:

$$C_{K^+}(\vec{r}) = C_{KCl}\exp\left[\frac{e\varphi(\vec{r})}{kT}\right] \quad (12)$$

$$C_{Cl^-}(\vec{r}) = C_{KCl}\exp\left[-\frac{e\varphi(\vec{r})}{kT}\right] \quad (13)$$

In this work, we apply the membrane voltage $V_m = \pm 1$ V to study how the membrane affects the capture and transport of nanoparticles. However, to simplify consideration and to focus on the membrane induced effects, we do not apply the electrolyte bias; thus, the main translocation mechanism of the nanoparticles is the (hindered) diffusion through the nanopore. When the electrolyte bias is present, two other transport mechanisms appear due to the electrphoresis and electroosmosis; their possible repercussions on the filtering of nanoparticles are briefly discussed in the Conclusion.

Brownian Dynamics. To describe the nanoparticle dynamics, we utilize the Brownian Dynamics (BD) approach.[41] In this approach, we first coarse-grain the simulated object; that is, we neglect its full atomic structure and replace it with a collection of suitably chosen and positioned beads while maintaining the total charge on the object. In case of a spherical nanoparticle, these beads are positioned in a simple cubic lattice, and each carries the same charge $q_i = -1e/N_b$, $i = 1, ..., N_b$, where N_b is the total number of beads. This charge distribution implies that the whole nanoparticle is uniformly charged with the total charge $-1e$. While this approach at first seems to be time-consuming and even redundant for a spherical uniformly charged nanoparticle (which can simply be treated as one bead of a given radius), it allows us future flexibility in describing other nanoscale objects with the nonuniform charge and density distribution such as proteins. The larger the number of beads, the more detailed description of the object's charge density is in principle possible. In this work, we placed beads in the nanoparticle at 0.3 nm apart, which means that the particle of diameter 3.2 nm (the largest considered in this work) has $N_b = 619$.

In the BD approach, the stochastic motion of the simulated object is usually described with the Langevin equation.[42] The crucial assumption of our BD model is the rigidity of the simulated object; that is, the beads once placed at their initial positions $\vec{\rho}_i$ do not change the distance with respect to the center of mass (COM) of the object. As such, we may consider the Brownian motion of the COM point only.

Thus, neglecting acceleration, we first discretize the translational Langevin equation that determines the COM position $\vec{R}(t)$ in the fixed system of reference connected with the membrane at time t as follows:

$$\vec{R}(t) = \vec{R}(t - \Delta t) - \sum_{i=1}^{N_b}\nabla_i U[\vec{r}_i(t - \Delta t)]\frac{\Delta t}{\xi} + \sqrt{\frac{6\Delta t k_B T}{\xi}}\vec{n} \quad (14)$$

where the second term on the right is the net force acting on the nanoparticle, $\xi = 6\pi\eta R_{nc}$ is the drag coefficient experienced by a spherical nanoparticle of radius R_{nc} moving in a solution with viscosity $\eta = 10^{-3}$ Pa s, $\Delta t = 0.5$ ps is the time increment of simulations, $T = 300$ K, and $k_B = 1.38 \times 10^{-23}$ J/K. The last term in this equation is the random force, which is responsible for the stochastic motion of the particle with $\vec{n}$ being the 3D random unit vector with components uniformly distributed in the interval [−1,1].

After determining $\vec{R}(t)$, the bead positions in the fixed frame, $\vec{r}_i$, are updated at each time step as

$$\vec{r}_i(t) = \vec{R}(t) + \vec{\rho}_i, \quad i = 1, ..., N_b \quad (15)$$

The potential energy $U(\vec{r}_i)$ of the individual bead in eq 14 has two contributions

$$U(\vec{r}_i) = U_m + q_i\varphi(\vec{r}_i) \quad (16)$$

corresponding, respectively, to the short-range Lennard-Jones (LJ) interaction energy due to the interaction between the beads and the membrane surface (U_m) and external electrostatic energy ($q_i\varphi$) due to charges in the semiconductor membrane and electrolyte.

To describe interaction with the membrane, instead of representing the membrane by a collection of atoms,[43,44] we use a continuous LJ potential:[12]

$$U_m = \varepsilon_m\left[\left(\frac{\sigma_m}{d_i}\right)^6 - 2\left(\frac{\sigma_m}{d_i}\right)^{12}\right] \quad (17)$$

where $\sigma_m = 2.5$ Å and $\varepsilon_m = 0.1$ kcal/mol are the equilibrium distance and the minimum value of the LJ potential, respectively, and d_i is the distance between the i-th bead and the nearest point on the membrane surface. In case of a chemically modified surface or a different chemical composition of the nanoparticle or the protein, it may be necessary to sample local regions of the membrane or the simulated particle to properly describe interaction between the studied object and the surface; this procedure can be easily incorporated in our model by modifying values of σ_m and ε_m accordingly.

Effect of the electrostatic interaction between the beads and charges in the membrane and on its surface is captured by the second term in eq 16 in which the electrostatic potential $\varphi(\vec{r}_i)$ is calculated from eq 9. As shown in the previous section, this long-range potential arises from the electrolyte charge, the static surface charge, bulk membrane dopant charges 9both fixed and mobile, see eqs 10 and 11), and the external membrane biases V_m, with the last two contributions being unique to our semiconductor membrane.

Conflict of Interest: The authors declare no competing financial interest.

Acknowledgment. This work was supported by the NSF grant CBET-1119446 and by the TeraGrid/XSEDE award for computational resources TG-PHY110023.

Supporting Information Available: A summary of approximations used in calculations as well as comparison with the electrostatic potential for SiO_2 membrane and proof-of-principle simulations of translocation for 10 nanoparticles. This material is available free of charge *via* the Internet at http://pubs.acs.org.

REFERENCES AND NOTES

1. Mochizuki, S.; Zydney, A. Theoretical Analysis of Pore Size Distribution Effects on Membrane Transport. *J. Membr. Sci.* **1993**, *82*, 211–228.
2. Striemer, C. C.; Gaborski, T. R.; McGrath, J. L.; Fauchet, P. M. Charge- and Size-Based Separation of Macromolecules Using Ultrathin Silicon Membranes. *Nature* **2007**, *445*, 749–753.
3. Venkatesan, B. M.; Bashir, R. Nanopore Sensors for Nucleic Acid Analysis. *Nat. Nanotechnol.* **2011**, *6*, 615–624.
4. Wei1, R.; Gatterdam, V.; Wieneke, R.; Tampe, R.; Rant, U. Stochastic Sensing of Proteins with Receptor-Modified Solid-State Nanopores. *Nat. Nanotechnol.* **2012**, *7*, 257–263.
5. Davenport, M.; Healy, K.; Pevarnik, M.; Teslich, N.; Cabrini, S.; Morrison, A.; Siwy, Z.; Letant, S. The Role of Pore Geometry in Single Nanoparticle Detection. *ACS Nano* **2012**, *6*, 8366–8379.
6. Miles, B. N.; Ivanov, A. P.; Wilson, K. A.; Dogan, F.; Japrung, D.; Edel, J. B. Single Molecule Sensing with Solid-State Nanopores: Novel Materials, Methods, and Applications. *Chem. Soc. Rev.* **2013**, *42*, 15–28.
7. Plesa, C.; Kowalczyk, S. W.; Zinsmeester, R.; Grosberg, A. Y.; Rabin, Y.; Dekker, C. Fast Translocation of Proteins through Solid State Nanopores. *Nano Lett.* **2013**, *13*, 658–663.
8. Kasianowicz, J.; Brandin, E.; Branton, D.; Deamer, D. Characterization of Individual Polynucleotide Molecules Using a Membrane Channel. *Proc. Natl. Acad. Sci. U.S.A.* **1996**, *93*, 13770–13773.
9. Dimitrov, V.; Aksimentiev, A.; Schulten, K.; Heng, J.; Sorsch, T.; Mansfield, W.; Miner, J.; Watson, G. P.; Cirelli, R.; Klemens, F.; *et al.* Exploring the Prospects for a Nanometer-Scale Gene Chip. *IEDM Tech. Dig.* **2006**, 169–173.
10. Gracheva, M. E.; Xiong, A.; Aksimentiev, A.; Schulten, K.; Timp, G.; Leburton, J.-P. Simulation of the Electric Response of DNA Translocation through a Semiconductor Nanopore-Capacitor. *Nanotechnology* **2006**, *17*, 622–633.
11. Gracheva, M. E.; Vidal, J.; Leburton, J.-P. p-n Semiconductor Membrane for Electrically Tunable Ion Current Rectification and Filtering. *Nano Lett.* **2007**, *7*, 1717–1722.
12. Melnikov, D. V.; Leburton, J.-P.; Gracheva, M. E. Slowing Down and Stretching Out DNA with an Electrically Tunable Nanopore in a *p-n* Semiconductor Membrane. *Nanotechnology* **2012**, *23*, 255501.
13. Liu, H.; Qian, S.; Bau, H. H. The Effect of Translocating Cylindrical Particles on the Ionic Current through a Nanopore. *Biophys. J.* **2007**, *92*, 1164–1177.
14. Jubery, T. Z.; Prabhu, A. S.; Kim, M. J.; Dutta, P. Modeling and Simulation of Nanoparticle Separation through a Solid-State Nanopore. *Electrophoresis* **2012**, *33*, 325–333.
15. German, S. R.; Luo, L.; White, H. S.; Mega, T. L. Controlling Nanoparticle Dynamics in Conical Nanopores. *J. Phys. Chem.* **2013**, *117*, 703–711.
16. Rohani, M. M.; Zydney, A. L. Role of Electrostatic Interactions during Protein Ultrafiltration. *Adv. Colloid Interface Sci.* **2010**, *160*, 40–48.
17. Snyder, J. L.; Clark, A.; Fang, D. Z.; Gaborski, T. R.; Striemer, C. C.; Fauchet, P. M.; McGrath, J. L. An Experimental and Theoretical Analysis of Molecular Separations by Diffusion through Ultrathin Nanoporous Membranes. *J. Membr. Sci.* **2011**, *369*, 119–129.
18. Pinto, S. I. S.; Miranda, J. M.; Campos, J. B. L. M. A Numerical Study of the Apparent Selectivity in the Fractionation of Two Macromolecules by Ultrafiltration. *Sep. Sci. Technol.* **2012**, *47*, 936–949.
19. Merchant, C.; Healy, K.; Wanunu, M.; Ray, V.; Peterman, N.; Bartel, J.; Fischbein, M. D.; Venta, K.; Luo, Z.; Johnson, A. T. C.; Drndic, M. DNA Translocation through Graphene Nanopores. *Nano Lett.* **2010**, *10*, 2915–2921.
20. Schneider, G. F.; Kowalczyk, S. W.; Calado, V. E.; Pandraud, G.; Zandbergen, H. W.; Vandersypen, L. M. K.; Dekker, C. DNA Translocation through Graphene Nanopores. *Nano Lett.* **2010**, *10*, 3163–3167.
21. Garaj, S.; Hubbard, W.; Reina, A.; Kong, J.; Branton, D.; Golovchenko, J. A. Graphene as a Subnanometre Trans-Electrode Membrane. *Nature* **2010**, *467*, 190–193.
22. Xie, P.; Xiong, Q.; Fang, Y.; Qing, Q.; Lieber, C. M. Local Electrical Potential Detection of DNA by Nanowire-Nanopore Sensors. *Nat. Nanotechnol.* **2011**, *7*, 119–125.
23. Jiang, Z.; Stein, D. Charge Regulation in Nanopore Ionic Field-Effect Transistors. *Phys. Rev. E* **2011**, *83*, 031203.
24. Gracheva, M. E.; Leburton, J.-P. Electrolytic Charge Inversion at the Liquid-Solid Interface in a Nanopore in a Doped Semiconductor Membrane. *Nanotechnology* **2007**, *18*, 145704–145710.
25. Kim, E.; Xiong, H.; Striemer, C.; Fang, D.; Fauchet, P.; McGrath, J.; Amemiya, S. A Structure-Permeability Relationship of Ultrathin Nanoporous Silicon Membrane: A Comparison with the Nuclear Envelope. *J. Am. Chem. Soc.* **2008**, *130*, 4230–4231.
26. Schuss, Z.; Singer, A.; Holcman, D. The Narrow Escape Problem for Diffusion in Cellular Microdomains. *Proc. Natl. Acad. Sci. U.S.A.* **2007**, *104*, 16098–16103.
27. Berezhkovskii, A. M.; Barzykin, A. V.; Zitserman, V. Y. Escape from Cavity through Narrow Tunnel. *J. Chem. Phys.* **2009**, *130*, 245104.
28. Note that this time is not the usual mean first passage time as the particle makes several attempts to permeate the membrane before finally succeeding, see Figure 2 in Supporting Information.
29. Biess, A.; Korkotian, E.; Holcman, D. Diffusion in a Dendritic Spine: The Role of Geometry. *Phys. Rev. E* **2007**, *76*, 021922.
30. Redner, S. *A Guide to First-Passage Processes*; Cambridge University Press: Cambridge, 2001.
31. Pagliara, S.; Schwall, C.; Keyser, U. F. Optimizing Diffusive Transport through a Synthetic Membrane Channel. *Adv. Mater.* **2013**, *25*, 844–849.
32. Brunn, P. O.; Fabrikant, V. I.; Sankar, T. S. Diffusion Through Membranes: Effect of a Nonzero Membrane Thickness. *Q. J. Mech. Appl. Math.* **1984**, *37*, 311–324.
33. Vlassiouk, I.; Apel, P. Y.; Dmitriev, S. N.; Healy, K.; Siwy, Z. S. Versatile Ultrathin Nanoporous Silicon Nitride Membranes. *Proc. Natl. Acad. Sci. U.S.A.* **2009**, *106*, 21039–21044.
34. Lee, P.-H.; Helms, V.; Geyer, T. Coarse-Grained Brownian Dynamics Simulations of Protein Translocation through Nanopores. *J. Chem. Phys.* **2012**, *137*, 145105.
35. Luan, B.; Aksimentiev, A. Control and Reversal of the Electrophoretic Force on DNA in a Charged Nanopore. *J. Phys.: Condens. Matter* **2010**, *22*, 454123.
36. Firnkes, M.; Redone, D.; Knezedic, J.; Doeblinger, M.; Rant, U. Electrically Facilitated Translocations of Proteins through Silicon Nitrade Nanopores: Conjoint and Competitive Action of Diffusion, Electrophoresis and Electroosmosis. *Nano Lett.* **2010**, *10*, 2162–2167.
37. Graf, P.; Nitzan, A.; Kurnikova, M.; Coalson, R. A Dynamics Lattice Monte Carlo Model of Ion Transport in Inhomogeneous Dielectic Enviroments: Method and Implementation. *J. Phys. Chem. B* **2000**, *104*, 12324–12338.
38. Chung, S. H.; Corry, B. Three Computational Methods for Studying Permiation, Selectivity and Dynamics in Biological Ion Channels. *Soft Matter* **2005**, *1*, 417–427.
39. Nikolaev, A.; Gracheva, M. Simulation of Ionic Current through the Nanopore in a Double-Layered Semiconductor Membrane. *Nanotechnology* **2011**, *22*, 165202.
40. Sze, S. M. *Physics of Semiconductor Devices*; John Wiley & Sons Ltd.: New York, 1981.

41. Slater, G. W.; Holm, C.; Chubynsky, M. V.; de Haan, H. W.; Dubé, A.; Grass, K.; Hickey, O. A.; Kingsburry, C.; Sean, D.; Shendruk, T. N.; *et al.* Modeling the Separation of Macromolecules: A Review of Current Computer Simulation Methods. *Electrophoresis* **2009**, *30*, 792–818.
42. Doi, M.; Edwards, S. F. *The Theory of Polymer Dynamics*; Clarendon Press: Oxford, 1999.
43. Fyta, M.; Melchionna, S.; Bernaschi, M.; Kaxiras, E.; Succi, S. Numerical Simulation of Conformational Variability in Biopolymer Translocation through Wide Nanopores. *J. Stat. Mech.* **2009**, *6*, 06009.
44. Bhattacharya, A.; Binder, K. Out-of-Equilibrium Characteristics of a Forced Translocating Chain through a Nanopore. *Phys. Rev. E* **2010**, *81*, 041804.